Supporting Information

Dakos *et al.* 10.1073/pnas.0802430105

SI Text

Derivation of Model-Simulated Data. Our simulated data presented in Fig. 2 come from three climate models of different complexity.

(*i*) We used a simple one-dimensional climate model (1, 2) to simulate a transition from a greenhouse to an icehouse Earth (Fig. 2*A*). The model has temperature, T, as the only state variable that represents the average temperature of an ocean on a spherical planet subjected to radiative heating (2) according to the equation:

$$\frac{dT}{dt} = \frac{1}{c}\left\{ -\varepsilon\sigma T^4 + \frac{1}{4}\mu I_0 bT + \frac{1}{4}\mu I_0(1-a)\right\}$$
$$\text{with } a_p = a - bT \qquad \textbf{[S1]}$$

where ε is effective emissivity, μ is relative intensity of solar radiation, I_0 is solar irradiance, c is a constant thermal inertia, and a_p is the planetary albedo. Parameters a and b define a linear feedback between ice and albedo variability and temperature. In this simple climate system, there is one internal equilibrium of nonglacial conditions, which, when I_0 drops below a certain threshold, there is a runaway effect to ice climate through a fold bifurcation.

We extended the deterministic skeleton of the model by including a stochastic term following the general form of a stochastic differential equation:

$$dx = f(x,\theta)dt + \sigma(x)dW, \qquad \textbf{[S2]}$$

where x is the state variable, f is the deterministic part of the model that depends on the control parameter θ, and σ scales the amount of noise that is introduced in the model with dW, a Wiener process. In this climate model, we used as control parameter the relative radiation μ. We produced a time series by decreasing the control parameter μ linearly with time from 1 to 0.9524, allowing a transition from a warm to a cold climate. We used σ equal to 0.003 (applied multiplicatively on the state variable) and all of the rest of the parameter values as they appear in ref. 2. We changed the original time scale of the model (= 1 sec) by rescaling time with a factor of $\delta = 20 \times 10^6$ (new time scale = 0.6342 years). Simulations were performed in MATLAB v.7.1.0246 by using an Euler–Murayama method to solve the stochastic equation with Ito calculus.

(*ii*) The thermo-haline circulation model simulation presented here is produced from the CLIMBER-2 model (3, 4), which is a coupled climate model of intermediate complexity. The ocean component originates from the module by Wright and Stocker (5). A freshwater forcing at 44° northern latitude is applied; the average forcing is superimposed with a Gaussian white noise time series. The 50,000 years transient run sees a linear increase in atmospheric CO_2 from 280 ppm to 800 ppm, implying an increased average freshwater forcing.

(*iii*) The deterministic climate model of the desertification of North Africa (Fig. 2*C*) (6) was extended by accounting for the synoptic component w_{syn} of vertical velocity w at the top of the planetary boundary layer:

$$w = w_m + w_h + w_{\text{syn}}$$
$$w_{\text{syn}} = \frac{K_T}{H_0}\left(k_{ts}^w \frac{\max(0, T_L - T_{cr})}{T_L^0 - T_{cr}} + k_{sl}^w \frac{T_L - T_B}{T_L^0 - T_B^0}\right)(1 + \xi(0,\sigma_w)) \qquad \textbf{[S3]}$$

and the synoptic component U_{syn} of the Hadley circulation potential U:

$$U = U_0 + U_{\text{syn}}$$
$$U_{\text{syn}} = k_{\text{syn}}^U U_0\left(1 + \frac{T_L - T_B}{T_L^0 - T_B^0}\xi(0,\sigma_U)\right) \qquad \textbf{[S4]}$$

which allows for the contribution from the synoptic-scale baroclinic and barotropic atmospheric eddies with characteristic time scales from 2 to 10 days. w_m is the vertical velocity in the mean monsoon circulation and w_h is the vertical velocity associated with the mean Hadley circulation, U_0 is the mean Hadley circulation potential, T_B and T_L are surface air temperature at the southern box boundary and over land, respectively, T_B^0 and T_L^0 are their reference values, K_T is a vertical macroeddy diffusion coefficient in the free troposphere, H_0 is a scale height for the atmospheric density, $\xi(0, \sigma_w)$ and $\xi(0, \sigma_U)$ are normally distributed stochastic variables with zero mean and variances σ_w and σ_U, respectively, and k_{ts}^w, k_{sl}^w and k_{syn}^U are model parameters that reflect partial contributions from the corresponding physical processes.

The terms $\frac{K_T}{H_0}k_{ts}^w\frac{\max(0,T_L - T_{cr})}{T_L^0 - T_{cr}}(1 + \xi(0,\sigma_w))$ and $\frac{K_T}{H_0}k_{sl}^w\frac{T_L - T_B}{T_L^0 - T_B^0}(1 + \xi(0,\sigma_w))$ in Eq. **S3** describe the components of the synoptic-scale vertical velocity perturbation attributed to tropical storms and squall lines, respectively. These parameterizations assume that tropical storms form when the temperature exceeds a critical threshold T_{cr} [assumed to be 26°C (7)], whereas the squall lines are mainly generated because of the lower troposphere wind shear in the African Easterly Jet associated with a temperature gradient $T_L - T_B$ between Sahara and the Gulf of Guinea (8). Parameters k_{ts}^w and k_{sl}^w were assigned 0.2 and 0.8, respectively, which reflects partial contributions to the synoptic-scale variability from the tropical storms and squall lines based on the empirical data (9, 10). The value of the variance σ_w was assigned 0.1 (11).

The synoptic term of the Hadley circulation potential (Eq. **S4**) includes a contribution from the synoptic variability, $k_{\text{syn}}^U U_0$, due to the synoptic-scale perturbations of the zonally averaged wind, and from the term associated with the local fluctuations of the Hadley circulation, which is assumed to be proportional to the local horizontal temperature gradient, $k_{\text{syn}}^U U_0\frac{T_L - T_B}{T_L^0 - T_B^0}\xi(0,\sigma_U)$. Parameters k_{syn}^U and σ_U were set equal to 0.05 and 0.1, respectively, based on empirical data (11).

Derivation of Paleoclimate Proxy Data. Because we were interested in measuring slowing down before the transition, we restricted our analysis to the period just before the transition in both simulated and proxy records. The exact parts of the original time series that we selected for our analysis, together with the size of the original record and data sources, are presented in supporting information (SI) Table S1. Because the exact selection of the part of the record is critical for the outcome of our analysis, we were careful to avoid points that were part of the transition. Because of increased serial correlation as the transition trend begins, including such points would bias the estimate of the AR(1) coefficient.

Data Analyses: Interpolation, Detrending, and Estimation of Autocorrelation at Lag 1. We applied the same analyses both to the simulated data and the real paleoclimate proxy records. Because the available paleoclimate data were of unequal density, we used linear interpolation to make our records equidistant (Table S3). However, as indicated in the main text, interpolation can create spurious trends in autocorrelation. A positive trend in autocorrelation could occur as an artifact of interpolation if the density of points would decrease toward the shift (and, hence, the role of interpolation would increase). Therefore, we checked the evolution of the time intervals in the original records and compared them with the equidistant time intervals of the interpolated records (Fig. S1). In general, the time intervals of the interpolated datasets were rather similar to the time intervals in the original time series close to the transition. Only in Fig. S1*a* (the end of greenhouse Earth), did the time between subsequent data points decrease toward the shift. However, this happened at the very end, and can therefore not be responsible for the long-term increasing autocorrelation trend detected. In any case, as shown in the next section, we analyzed the sensitivity of our results to interpolation systematically for all time series.

We removed slow trends in the original records by applying a Gaussian kernel smoothing function [based on the Nadaraya–Watson kernel regression estimate (12)] over the interpolated record before the transition and subtracted it from the interpolated record to obtain the residual time series (Fig. S2). The choice of the size of the bandwidth is important in this process. We picked bandwidths such that we do not overfit our data but yet filter out the slower trends in the records.

In ref. 13 changes in power spectra were used as an indicator for the proximity to thresholds, tested in a 1D model of the thermohaline circulation of the North Atlantic. The spectrum is equivalent to the full autocorrelation function. Here, according to ref. 14, the spatial dynamics become degenerate at the transition, leading to the observation of the critical mode in arbitrary generic 1D time series. By assuming time-scale separation at the bifurcation, we can use only the first entry of the autocorrelation function, that is, the lag-1 information; in that sense, the current method is more parsimonious. To calculate the autocorrelation at lag 1, which is an estimator of the slowing down of the system (15), we fitted an autoregressive model of order 1 (AR1) on data that are included within a sliding window of half the size of the record before the transition. The AR1 *ansatz* (14) is of the form $x_{t+1} = \alpha_1 x_t + \varepsilon_t$, fitted by an ordinary least-squares method (OLS) with Gaussian random error ε_t. Note that we calculated no intercept, because we are fitting the AR1 model on the detrended residuals with mean zero. Although there have been modifications to the AR1 *ansatz* (16) where the authors used detrended fluctuation analysis (DFA), we used the degenerate fingerprinting approach (14) because of its most direct relation to generic bifurcations and straightforward applicability.

Finally, to determine the evolution of the AR1 estimates before the transition we used the nonparametric Kendall τ rank correlation coefficient to check against the null hypothesis of randomness for a sequence of measurements against time (17).

All analyses were implemented in MATLAB v7.1.0246 (Mathworks) and in Rv2.4.1 (R project for Statistical Computing). Specifically, we used (*i*) for the linear interpolation, the function *interp1* (MATLAB); (*ii*) for the detrending of the records, the function *ksmooth* (R); (*iii*) for the estimates of the autoregressive coefficients, the function *ar.ols* (R); and (*iv*) for the calculation of the trend statistic, the function *cor.test* (R) for the Kendall τ correlation statistics together with the *P* values (two-tailed with $\alpha = 0.05$).

Effect of Interpolating on the Results. We also explored the estimates of our trend statistic on the original records without interpolating missing values. Obviously, working with nonequidistant data violates the basic assumptions behind time series analysis. However, we pursued it only as an extra check on the robustness of our results. Thus, we treated the original time series as equidistant, we removed the slow trends (using the same bandwidth for the Gaussian filter as we did in their interpolated counterparts), and we estimated the autoregressive coefficients at lag 1 within a sliding window of half the size of the time series. In all eight cases, our positive trend from the interpolated records are similar to those from the original time series (Table S3). In all cases the trend statistic was of the same order of magnitude, and although there were three cases where interpolated records yielded a stronger increase in the AR(1) coefficient than the noninterpolated ones (end of greenhouse Earth, end of Younger Dryas, and end of glaciation II), there were three other cases where the opposite was observed (end of glaciation I, III, and Bølling–Alleröd) and one in which there was no real difference (glaciation IV).

Analysis of Surrogate Time Series. To test for the likelihood of obtaining estimates of trend statistics by randomness, we created surrogate time series by three different ways.

(*i*) We bootstrapped our datasets by reshuffling the order of the detrended original time series and by picking data with replacement to generate surrogate records of similar probability distribution (mean and variance) (18) (H_0 1).

(*ii*) We produced surrogate time series with the same autocorrelations and the same probability distribution as the data, to test against the H_0 hypothesis that our datasets are a realization of a Gaussian linear stochastic process (19, 20) (H_0 2). We did this by replicating data of the same Fourier spectrum and amplitudes as of the original set using the MATLAB function *generate_iAAFT* (21).

(*iii*) To test against the H_0 hypothesis that the data are produced by a colored-noise process with similar variance, mean, and autocorrelation at lag 1 with the original detrended time series (22) (H_0 3), we generated surrogate sets by an AR1 model $x_{t+1} = \alpha_1 x_t + \alpha_0 + \sigma\varepsilon_t$, where $\alpha_1 = A(1)$, $\sigma^2 = v(1 - \alpha_1^2)$, $\alpha_0 = \mu(1 - \alpha_1)$, with v the variance, μ the mean, $A(1)$ the autocorrelation at lag 1 from the residual time series (estimated by using function *acf* as implemented in *R*), and σ a scaling factor for the Gaussian random error ε_t.

We estimated the probability that our estimates of the trend statistic would be observed by chance as the fraction of the 1,000 surrogate series scoring the same value or a higher one. Specifically for the Kendall τ, we estimated this probability as the number of cases in which the statistic was equal to or higher than the estimate of the original record, $P(\tau \geq \tau^*)$. We also estimated the combined probability for observing the trend statistic estimate in each the H_0 hypotheses test by chance. For this, we used the Fisher's combined probability test (23) to estimate the X^2 statistic, given by:

$$X^2_{2k} = -2\sum_{i=1}^{k} \ln(p_i) \qquad \text{[S5]}$$

where k is the amount of tests (here, $k = 8$) and P is the probability estimated for each H_0 hypotheses test (Table S2). The combined probability for the X^2 statistic was given by a χ^2 distribution with $2k$ degrees of freedom.

The probability estimates for the model and data trend statistic under the three different H_0 hypotheses are shown in Table S2. The probability of, by chance, acquiring a similar trend estimate as in the original record differs from case to case. In the case of the models, the probabilities were consistently very low ($P < 0.05$). Similarly low probabilities were estimated in the records of the transitions of the greenhouse Earth, the Younger

Dryas and the glaciation I (Fig. S3). In the shorter time series the probabilities of finding the observed trends by chance is much higher. Nonetheless the combined probability of finding positive trends in all eight data series is obviously very low (lower row Table S2).

Robustness Against Choice of Window Size and Filtering Resolution. The results of our analyses are obviously influenced by the standard deviation (defined by bandwidth size) used in the kernel function for filtering and the size of the sliding window used to compute autocorrelation. In the latter there is a trade-off between time resolution and reliability of the estimate. Smaller windows allow one to track short-term changes in autocorrelation. However, the small number of data points in the window makes the estimate of autocorrelation less reliable. The filtering poses another trade-off. A too-wide filter does not remove slow trends that may lead to spurious autocorrelation. Especially, at the ends of the time series the deviation becomes obvious if a too-wide kernel size is used. A too-narrow filter removes the short-term fluctuations that we intend to study for signs of slowing down. A systematic sensitivity analysis for our three longest time series and the model results indicate that the results are quite robust, and that actually we could have obtained more significant trends by tuning the parameters for the specific series (Fig. S4).

1. Fraedrich K (1979) Catastrophes and resilience of a zero-dimensional climate system with ice-albedo and greenhouse feedback. *Q J R Meteorol Soc* 105:147–167.
2. Fraedrich K (1978) Structural and stochastic analysis of a zero-dimensional climate system. *Q J R Meteorol Soc* 104:461–474.
3. Ganopolski A, *et al.* (2001) CLIMBER-2: A climate system model of intermediate complexity. Part II: model sensitivity. *Clim Dyn* 17:735–751.
4. Petoukhov V, *et al.* (2000) CLIMBER-2: A climate system model of intermediate complexity. Part I: model description and performance for present climate. *Clim Dyn* 16:1.
5. Stocker TF, Wright DG, Mysak LA (1992) A zonally averaged, coupled ocean atmosphere model for paleoclimate studies. *J Clim* 5:773–797.
6. Brovkin V, Claussen M, Petoukhov V, Ganopolski A (1998) On the stability of the atmosphere-vegetation system in the Sahara/Sahel region. *J Geophys Res* 103:31613–31624.
7. Gray WM (1968) Global view of origin of tropical disturbances and storms. *Mon Weather Rev* 96:669–679.
8. Cook KH (1999) Generation of the African easterly jet and its role in determining West African precipitation. *J Clim* 12:1165–1184.
9. Grist JP, Nicholson SE (2001) A study of the dynamic factors influencing the rainfall variability in the West African Sahel. *J Clim* 14:1337–1359.
10. Joseph E, *et al.* (2003) Paper presented at the First International GPM GV Requirements Workshop, Cosenors House, Abington, UK, 4–7 November 2003.
11. Petoukhov V, Eliseev AV, Klein R, Oesterle H (2007) On statistics of the free-troposphere synoptic component: an evaluation of skewnesses and mixed third-order moments contribution to the synoptic-scale dynamics and fluxes of heat and humidity. *Tellus A,* 10.1111/j.1600-0870.2007.00276.
12. Hastie TJA, Tibshirani RJ (1990) Generalized Additive Models, Monographs on statistics and applied probability (Chapman & Hall, London).
13. Kleinen T, Held H, Petschel-Held G (2003) The potential role of spectral properties in detecting thresholds in the Earth system: application to the thermohaline circulation. *Ocean Dyn* 53:53–63.
14. Held H, Kleinen T (2004) Detection of climate system bifurcations by degenerate fingerprinting. *Geophys Res Lett* 31:L23207.
15. van Nes EH, Scheffer M (2007) Slow recovery from perturbations as a generic indicator of a nearby catastrophic shift. *Am Nat* 169:738–747.
16. Livina VN, Lenton TM (2007) A modified method for detecting incipient bifurcations in a dynamical system. *Geophys Res Lett* 34:L23207.
17. Mann HB (1945) Nonparametric tests against trend. *Econometrica* 13:245–259.
18. Efron B, Tibshirani R (1986) Bootstrap methods for standard errors, confidence intervals, and other measures of statistical accuracy. *Stat Sci* 1:54–77.
19. Schreiber T, Schmitz (1996) A improved surrogate data for nonlinearity tests. *Phys Rev Lett* 77:635.
20. Schreiber T, Schmitz A (2000) Surrogate time series. *Physica D Nonlinear Phenomena* 142:346–382.
21. Gautama T, Mandic DP, Van Hulle MM (2004) A novel method for determining the nature of time series. *IEEE Trans Biomed Eng* 51:728–736.
22. Theiler J, Eubank S, Longtin A, Galdrikian B, Farmer JD (1992) Testing for nonlinearity in time-series—The method of surrogate data. *Physica D* 58:77–94.
23. Sokal RR, Rohlf FJ (1995) *Biometry: The principles and Practice of Statistics in Biological Research* (Freeman, New York), 3rd Ed.
24. Tripati A, Backman J, Elderfield H, Ferretti P (2005) Eocene bipolar glaciation associated with global carbon cycle changes. *Nature* 436:341–346.
25. Hughen KA, Southon JR, Lehman SJ, Overpeck JT (2000) Synchronous radiocarbon and climate shifts during the last deglaciation. *Science* 290:1951–1954.
26. Alley RB (2000) The Younger Dryas cold interval as viewed from central Greenland. *Q Sci Rev* 19:213–226.
27. deMenocal P, Ortiz J, Guilderson T, Sarnthein M (2000) Coherent high- and low-latitude climate variability during the holocene warm period. *Science* 288:2198–2202.
28. Petit JR, *et al.* (1999) Climate and atmospheric history of the past 420,000 years from the Vostok ice core, Antarctica. *Nature* 399:429–436.

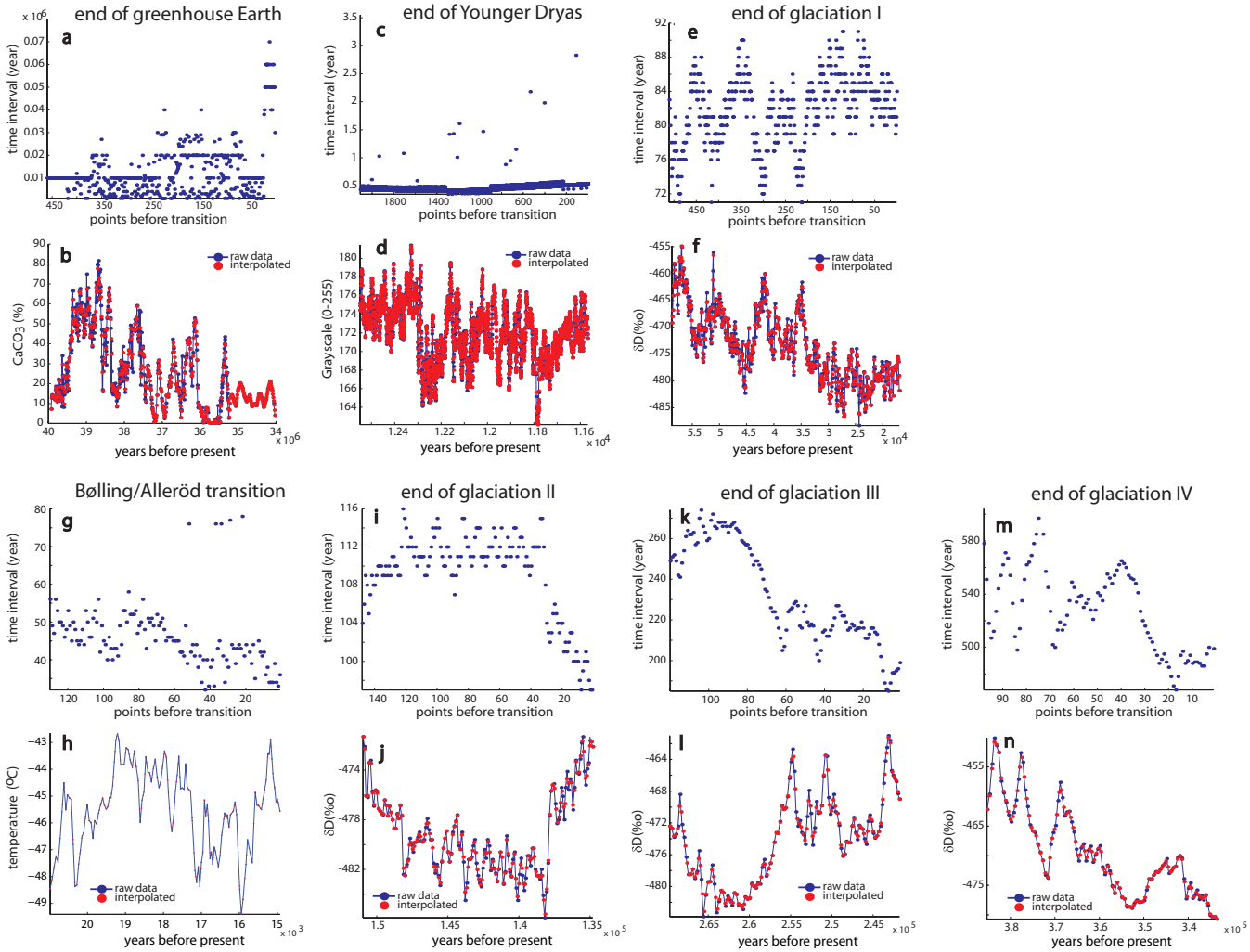

Fig. S1. Plots of time intervals and interpolated data. (*a, c, e, g, i, k,* and *m*) Plots of time intervals over proximity to the transition in the original records shown in the main text (Fig. 1). Time intervals are estimated in time units of years by differencing the times at which the data were dated. Smaller time intervals indicate increased density of points. In all cases, except from *a*, the time intervals close to the transitions in the original records are of similar magnitude to the time interval of the interpolated datasets (compare with Table S3). (*b, d, f, h, j, l,* and *n*) Plots of the interpolated data (red points) superimposed on the original records (blue points).

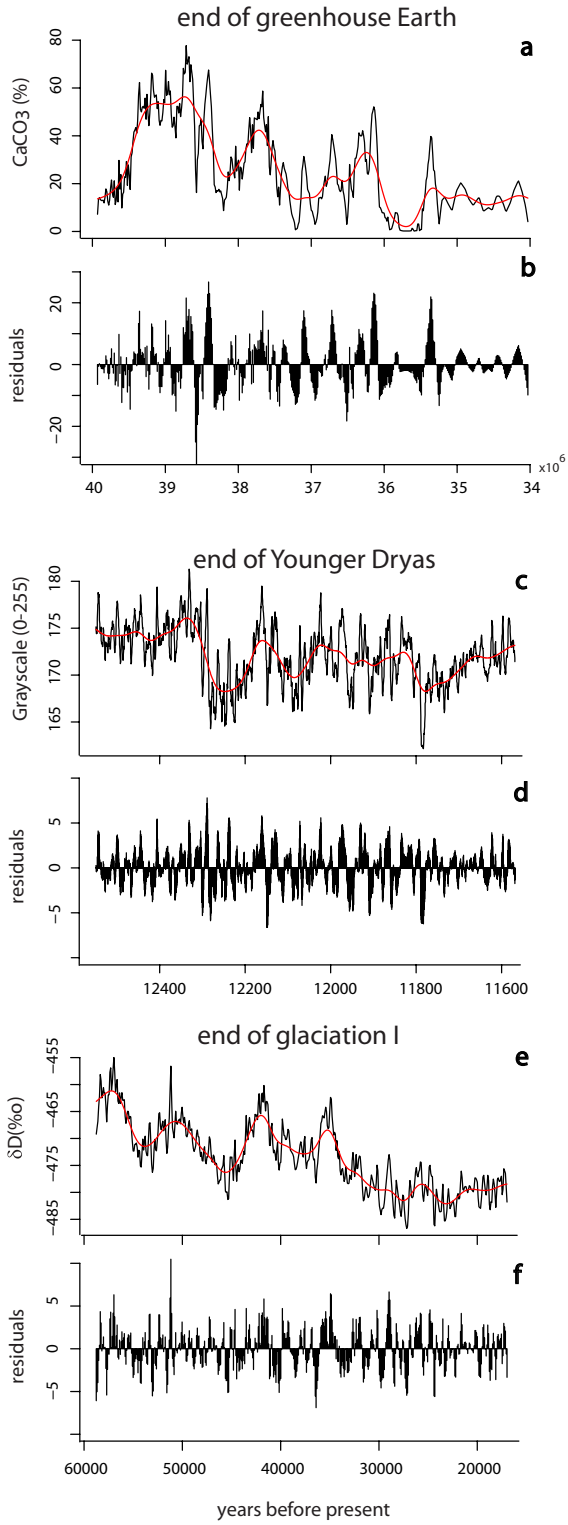

Fig. S2. Effects of filtering on the records shown in Fig. 1 in the main text. (*a*, *c*, and *e*) Data points before the transition and the Gaussian kernel filter used for detrending. (*b*, *d*, and *f*) The residual time series after subtracting the trend (red line). Records shown correspond to the records depicted in Fig. 1 in the main text.

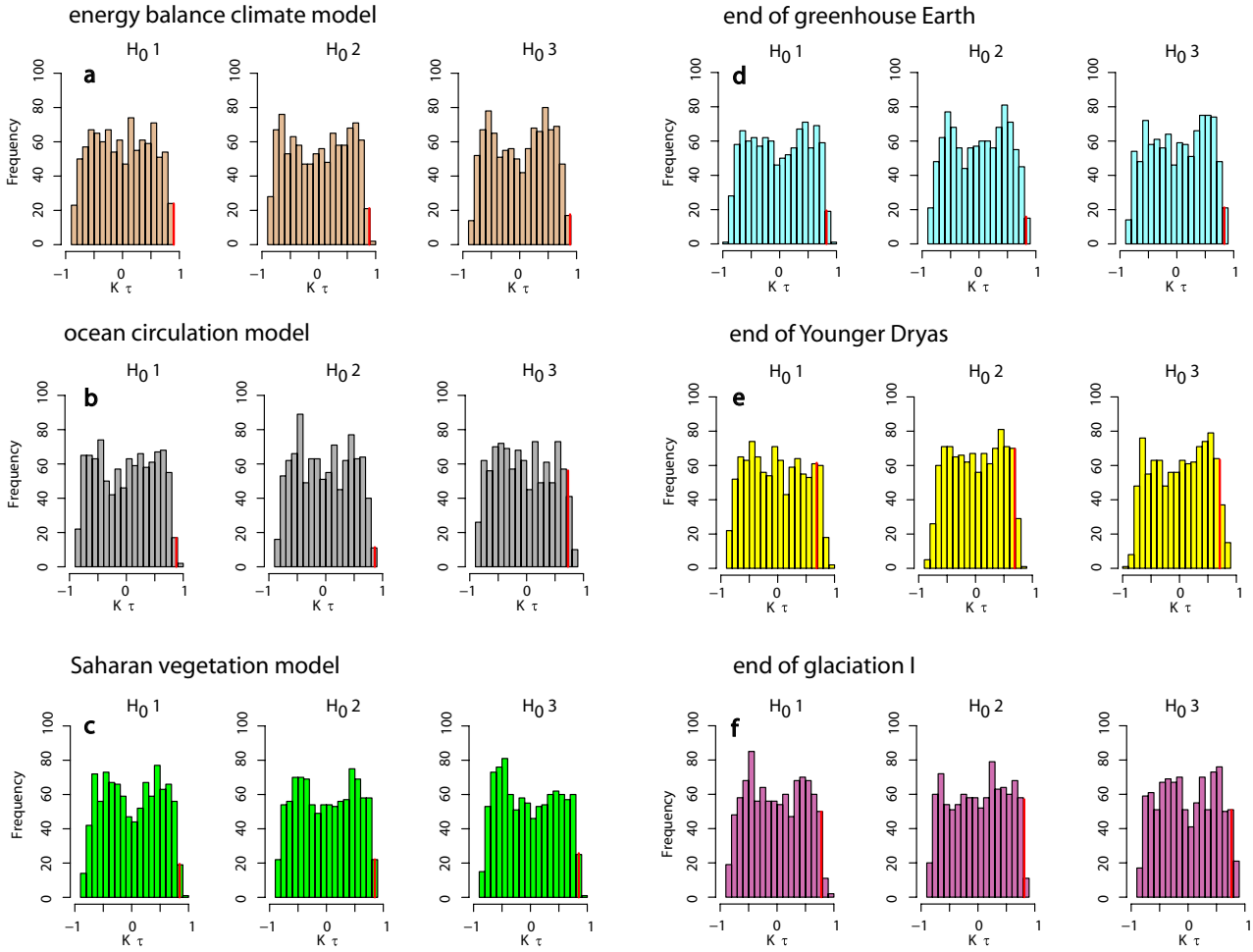

Fig. S3. Probability distributions of the estimated trend statistic (Kendall's τ) of the ranked order test, under three alternative H_0 hypotheses for a set of 1,000 surrogate time series. Under H_0 1, datasets are generated after bootstrapping the residual time series records, under H_0 2 new datasets are produced with similar distribution and Fourier spectra as the residual time series, and under H_0 3 the surrogate time series have been produced from an autoregressive model with similar autocorrelation at lag 1, mean, and variance as in the residual records. Red lines indicate the limit over which the surrogate trend statistic is higher than the trend statistic of the original residual records. From this subset, only values of significance *P* equal to or higher than the original record are used to estimate the likelihood of acquiring trend statistic estimates of similar magnitude.

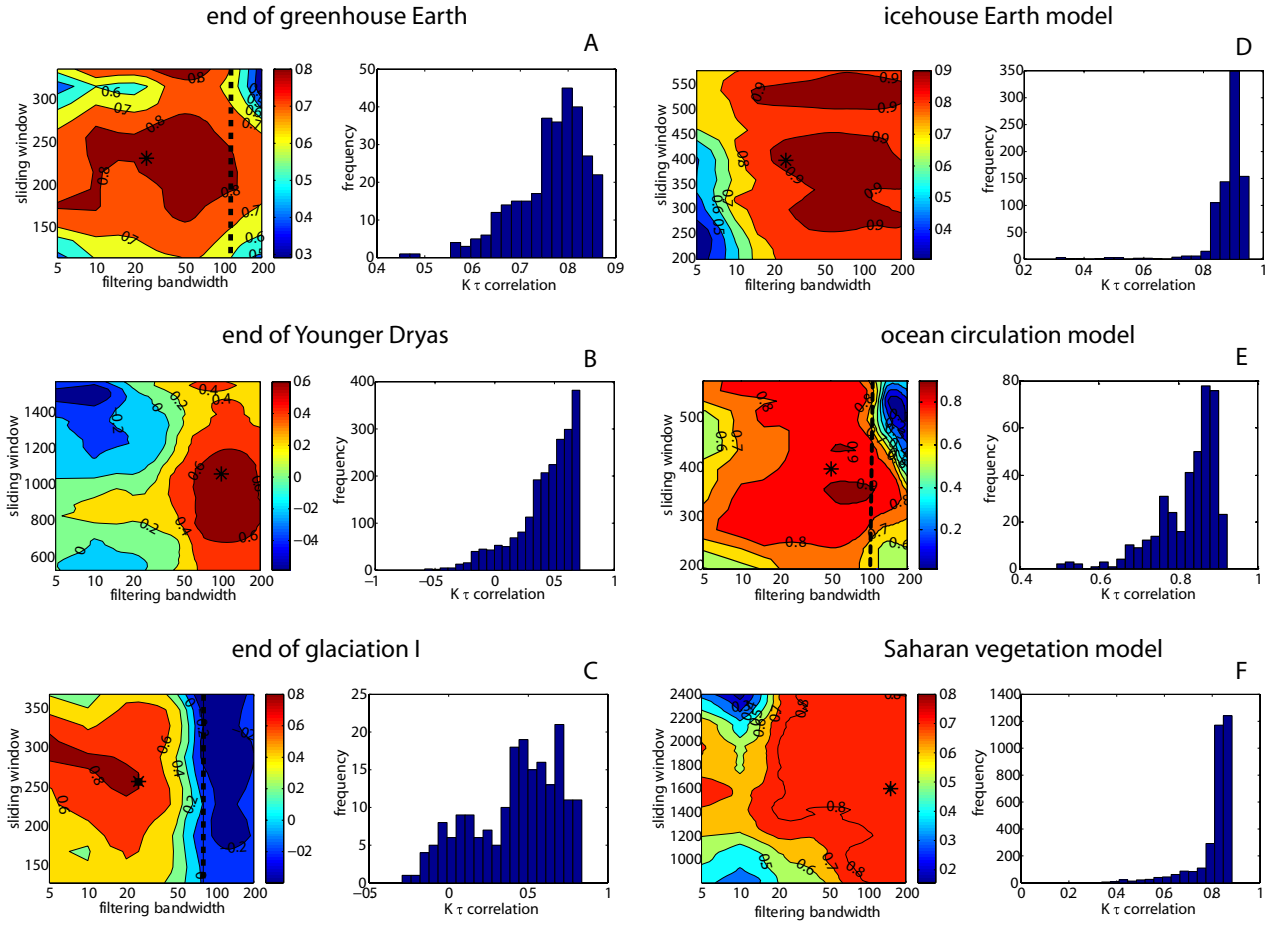

Fig. S4. Contour plots show the effect of the width of the sliding window and the width of the kernal filter on the observed trend in autocorrelation for the climate original data and simulated results shown in the main text as measured by the Kendall's τ. Stars indicate the parameter choice used in the analyses presented in the text. We visually inspected the fit of the kernel filter line to the data and demarcated where the kernel width becomes too large to follow the trend in the data (dashed vertical lines in some contour plots). The histograms give the frequency distribution of the trend statistic for the scanned parameter area to the left hand side of the dashed line.

Table S1. Paleoclimate records together with their origin, the proxy measured, the approximate range, and transition threshold used in the analyses, as well as the dataset citation and the original reference of the record

Paleo record	Origin	Climate proxy (units)	Time range, yrs BP	Time of transition	*N*	Dataset	Original reference
End of greenhouse Earth	ODP tropical Pacific core 1218	$CaCO_3$ (%)	(39–32) $\times$ 10^6	34 $\times 10^6$	482	*	24
Bølling-Alleröd transition	GISP2 ice core	Temperature (°C)	21,000–14,600	15,000	147	†	25
End of Younger Dryas	Cariaco basin core PL07–58PC	Grayscale (0–255)	12,500–11,200	11,600	2652	‡	26
Desertification of North Africa	ODP Hole 658C	Terrigenous dust (%)	8,300–4,800	7,500	40	§	27
End of glaciation I	Vostok ice core	d2H (%)	58,800–12,000	17,000	591	¶	28
End of glaciation II	Vostok ice core	d2H (%)	151,000–128,000	135,000	258	¶	28
End of glaciation III	Vostok ice core	d2H (%)	270,000–238,000	242,000	149	¶	28
End of glaciation IV	Vostok ice core	d2H (%)	385,300–324,600	334,100	126	¶	28

*Tripati A, *et al.* (2005). Eocene Greenhouse-Icehouse Transition Carbon Cycle Data. IGBP PAGES/World Data Center for Paleoclimatology Data Contribution Series no. 2005-056. NOAA/NGDC Paleoclimatology Program, Boulder CO.

†Alley R (2004) GISP2 Ice Core Temperature and Accumulation Data. IGBP PAGES/World .Data Center for Paleoclimatology Data Contribution Series no. 2004-013. NOAA/NGDC Paleoclimatology Program, Boulder CO.

‡Hughen K, *et al.* (2000) Cariaco Basin 2000 Deglacial 14C and Grey Scale Data, IGBP PAGES/World Data Center A for Paleoclimatology Data Contribution Series no. 2000-069.NOAA/NGDC Paleoclimatology Program, Boulder CO.

§deMenocal PB, *et al.* (2001) Holocene Variations in Subtropical Atlantic SST. IGBP PAGES/World Data Center A for Paleoclimatology Data Contribution Series no 2001-054. NOAA/NGDC Paleoclimatology Program, Boulder CO.

¶Petit JR, *et al.* (2001) Vostok Ice Core Data for 420,000 Years, IGBP PAGES/World Data Center for Paleoclimatology Data Contribution Series no. 2001-076. NOAA/NGDC Paleoclimatology Program, Boulder CO.

Table S2. Probability of acquiring the estimated values for the trend statistic (Kendall's τ) of the original and simulated residual time series under three alternative H_0 hypotheses for a set of 1,000 surrogate time series

(N = 1000 surrogate sets)	H_0 1	H_0 2	H_0 3
Original record (residuals)	Kendall τ	Kendall τ	Kendall τ
End of greenhouse Earth	0.014**	0.004**	0.011**
End of Younger Dryas	0.086*	0.03**	0.055*
End of glaciation I	0.013**	0.011**	0.021**
Bølling–Alleröd transition	0.367	0.340	0.332
End of glaciation II	0.402	0.397	0.386
End of glaciation III	0.247	0.235	0.234
End of glaciation IV	0.186	0.043**	0.125
Desertification of North Africa	0.140	0.165	0.091*
Fisher's combined probability	*0.002847*	*0.000206*	*0.001278*
Simulated record (residuals)			
Energy balance climate model	$<10^{-4}$**	0.002**	$<10^{-4}$**
Saharan vegetation model	0.002**	0.001**	0.006**
Ocean circulation model	0.003**	$<10^{-4}$**	$<10^{-4}$**

Under H_0 1, datasets are generated after bootstrapping, under H_0 2 new data sets are produced with similar distribution and Fourier spectra as the residual time series, and under H_0 3 the surrogate time series have been produced from a autoregressive model with similar autocorrelation at lag 1, mean, and variance as in the residual records. *, $P \leq 0.1$. **, $P \leq 0.05$. In italics, the combined probability for obtaining the estimated probabilities for each hypothesis is provided.

Table S3. Summary of trend statistic for the original (noninterpolated) and interpolated paleo records, and their probabilities (*P*)

Record	*N* points original/ interpolated	Bandwidth size	Original K τ (*P*)	Interpolated K τ (*P*)
End of greenhouse Earth	461/462	25	0.5 ($<10^{-4}$)	0.83 ($<10^{-4}$)
End of Younger Dryas	2,110/2,111	100	0.34 ($<10^{-4}$)	0.69 ($<10^{-4}$)
End of glaciation I	512/513	25	0.85 ($<10^{-4}$)	0.8 ($<10^{-4}$)
Bølling–Alleröd transition	131/132	25	0.37 ($<10^{-4}$)	0.27 (0.001)
End of glaciation II	149/150	25	0.08 (0.31)	0.17 (0.27)
End of glaciation III	121/122	10	0.67 ($<10^{-4}$)	0.43 ($<10^{-4}$)
End of glaciation IV	99/100	50	0.51 ($<10^{-4}$)	0.52 ($<10^{-4}$)
Desertification of North Africa	88/88*	10	0.58 (0.001)	0.58 (0.001)

*In the case of the desertification of North Africa the original data were already interpolated.